Initial stages of heteroepitaxial Mg growth on W(110): Early condensation, anisotropic strain, and self-organized patterns

L. Aballe,* A. Barinov, A. Locatelli, T. O. Mentes, and M. Kiskinova
ELETTRA-Sincrotrone Trieste, S. S. 14-km 163,5, Area Science Park, 34012 Basovizza, Trieste, Italy
(Received 19 October 2006; published 14 March 2007)

We have studied the initial stages of the heteroepitaxy of Mg on W(110) *in situ*, by means of complementary microscopic and spectromicroscopic techniques. In the submonolayer coverage regime the Mg film undergoes a series of structural transitions which are clearly distinguished in the diffraction pattern. Monitoring the Mg 2*p* core-level permits the identification of the different energy shifts associated with each superstructure. During deposition of the second Mg monolayer at moderate temperatures, the growth of single atomic height stripes is observed. The Mg 2*p* core level of the first (interface) and second monolayer are remarkably separated. The density, length, and width of the stripes, stabilized by the anisotropic misfit between the W(110) and Mg(0001) lattices, can be tuned by modifying the growth parameters.

DOI: 10.1103/PhysRevB.75.115411 PACS number(s): 68.55.−a, 73.20.At, 79.60.Dp, 68.37.Nq

I. INTRODUCTION

There is an ongoing effort to creating surface-supported low-dimensional structures of metals, semiconductors, and insulators. Common strategies in fabrication of such low-dimensional structures at surfaces are essentially based on growth phenomena. Films of only a few atomic layer thickness, micro- and nanoscopic wires, and islands can be obtained by self-organized growth attained by controlling the deposition and diffusion rates on the surface during homo- or heteroepitaxy. The structural, electronic, and magnetic properties of the low-dimensional structures may strongly differ from those of the corresponding bulk materials. On one hand their atomic structure might be subject to distortions through strain or pseudomorphism due to the interaction with the substrate or a growth far from thermodynamic equilibrium. On the other hand, the reduced dimensions can lead to strongly modified electronic properties due to electron confinement or hybridization with the substrate. Often the density of states near the Fermi level can be very different from that of the bulk, and can be tailored to a certain extent by choosing the appropriate system and morphology. Ultrathin metal films have been a subject of intense research during the last few years[1] since they provide a laboratory for basic quantum-mechanical concepts, and find applications in the microelectronic industry, especially in magnetic data storage technology. Ultrathin films of simple metals have also been shown to present nonmetal to metal transitions in the lowest coverage limit,[2] as well as unique collective phenomena that can strongly influence their photoresponse.[3]

Magnesium is a simple, free-electron-like but, nonetheless, reactive metal. It can be grown in perfect epitaxial overlayers on Si[4] and W(110),[5,6] presenting a splitting of the *s-p* valence band into thickness-dependent quantum-well states due to electron confinement within the overlayer. The Mg/W(110) system has a sharp interface with a high reflectivity in the energy region of the Mg *s-p* band and has proven an excellent test system to study the influence of confinement on the electronic structure[5] and on metal properties such as the surface reactivity.[6]

We have studied the initial stages of Mg/W(110) epitaxy, starting from the initial adatom adsorption and up to multilayer films by a combination of microscopic structural and spectroscopic techniques. This comprehensive analysis permits identification of an interesting variety of coverage dependent submonolayer phases, each one associated with a particular Mg core-level energy, resulting from the competition between the interaction with the substrate and the attractive Mg-Mg interaction. Furthermore, uniaxial strain in the interface Mg layer due to anisotropic misfit with the substrate lattice leads to the self-organized formation of atomic height mesoscopic wires during growth of the second atomic layer. This results in alternating two-monolayer (ML) stripes with nearly relaxed surface layer on a strongly strained Mg monolayer, with a distinct energy shift of the Mg 2*p* core level. The morphology of the striped phase is extremely sensitive to the growth parameters and might be used in future model adsorption studies.

II. EXPERIMENTAL DETAILS

We have studied simultaneously the morphology, chemical identity, and valence structure of ultrathin Mg/W(110) films for different growth conditions, using the SPELEEM microscope in operation at the Nanospectroscopy beamline at Elettra.[7] The microscope can perform several complementary techniques such as low-energy electron microscopy (LEEM) and x-ray photoemission electron microscopy (XPEEM) at high spatial and energetic resolution, as well as microspot low-energy electron diffraction (μLEED), x-ray photoelectron spectroscopy (μXPS), or photoelectron diffraction (μPED). In short, LEEM permits studying the evolution of the film morphology in real time, with 10 nm lateral and atomic depth resolution. With photoelectron microscopy the substrate and overlayer core levels and valence band can be measured with a spatial resolution down to 30 nm.

The W(110) substrate was cleaned by cycles of oxidation and flashing to 1800 K. Mg was evaporated from an Omicron electron-beam evaporator, at evaporation rates around 0.1 ML/min. We will refer to the deposition rates and submonolayer coverages (θ) in terms of the saturated interface Mg monolayer, which has an atomic density of 1.24

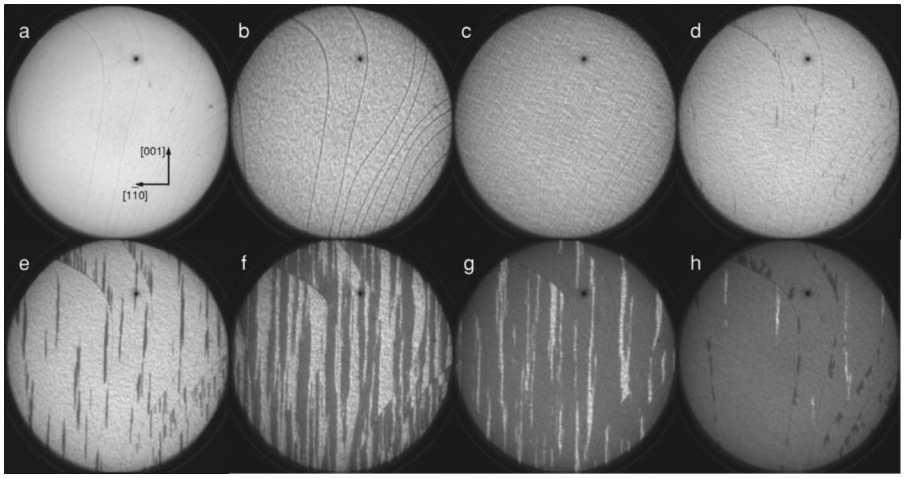

FIG. 1. Sequence of LEEM images as a function of Mg coverage, during growth at 405 K and deposition rate slightly below 0.1 ML/min. The field of view is 5 μm, the electron energy is 5 eV (a)–(c) and 11.1 eV (d)–(h). Mg coverages are 0, 0.03, 0.5, 1, 1.1, 1.5, 1.8, and 2 MLs.

$\times 10^{15}$ cm^{-2} [10.4% denser than the relaxed Mg(0001) planes]. The W(110) substrate was maintained between room temperature and 450 K for the different experiments.

The photoemission spectra presented were measured in μXPS mode. This is done by selecting the photoelectrons from a 3 μm^2 area and imaging the dispersive plane (exit of the energy analyzer) on the microchannel plate of the microscope. The spectra, acquired as snapshots of the energy dispersive plane with a charge-coupled device camera, are corrected for inhomogeneities in the channel plate response before further analysis. The core levels are fitted with Doniach-Sunjic spin-orbit doublets using the FitXPS package.[8]

III. RESULTS AND DISCUSSION

The coverage dependent atomic and electronic structure of the initial Mg adsorption on the W(110) surface has been studied at different temperatures, revealing a rich variety of morphologies with characteristic electronic structures. Growth of Mg proceeds layer by layer from room temperature up to 450 K. Above this temperature multilayer desorption takes place leaving behind the interface Mg monolayer, which does not desorb completely up to ≈700 K. Already at about 400 K we have observed slow desorption of Mg in excess of 1 ML, in a layer by layer fashion, but multilayer films can be grown in supersaturation conditions, i.e., increasing the deposition rate, and "freezing" the film after the desired morphology is reached. On the other end, at room temperature, growth is exactly layer by layer, with nucleation in areas below 10 nm (i.e., no structure is distinguished in LEEM). Photoelectron spectroscopy has shown that highly perfect films can be grown at room temperature up to at least 80 ML Mg.[5]

In all the temperature ranges, the Mg-W interaction stabilizes a strongly strained interface Mg lattice with a clear fingerprint of the substrate symmetry. In the narrow temperature window between 350 and 450 K, the formation of one-dimensional stripes of the second Mg monolayer on top of the anisotropically strained wetting monolayer is observed. The competing kinetics of adsorption, desorption, and anisotropic adatom diffusion permits varying the density, aspect ratio, and size of these mesoscopic wires by slight variations of the growth conditions.

A. Structural overlayer evolution during initial growth of Mg on W(110)

1. LEEM

The growth of the interface Mg layer on W(110) as seen by LEEM is illustrated in Figs. 1(a)–1(d). These images are extracted from a deposition series at 405 K, but the general features are qualitatively the same for substrate temperatures between 350 and 450 K. At first, images of the clean substrate present only large W(110) terraces separated by monoatomic steps [Fig. 1(a)]. As soon as Mg deposition begins, there is a sharp decrease in the electron reflectivity. In a very narrow coverage range (0.01–0.06 MLs), the contrast at steps edge is enhanced, and they appear thicker, indicating condensation of Mg at steps. This is either accompanied ($T<\sim 400$ K) or immediately followed ($T>\sim 400$ K) by the development of a grainy aspect of the terraces, indicating that Mg condensation takes place also on them [Fig. 1(b)]. From about 0.1 ML, contrast at step-edges becomes weaker and no sharp structures are distinguishable within the terraces [Fig. 1(c)], while the drop in the reflectivity continues up to ≈0.15 ML, indicating a disordered disperse phase. Above 0.15 ML, there is a smooth intensity increase, while typically small inhomogeneities are visible on the terraces. It will be shown that in this coverage range, ordered islands coexist with the dispersed phase, covering an increasingly larger fraction of the surface. As shown in Fig. 1(d), upon monolayer completion, steps become clearly visible again, mimicking the substrate step topography.

Immediately after completion of the first monolayer, excess Mg nucleates as thin and long needles, extending along the bcc[001] direction. The spontaneous growth of microscopic single atomic height wires, visible as dark areas on the bright 1 ML background, is illustrated in Figs. 1(d)–1(h). In Fig. 1(d), the first Mg monolayer completely covers the substrate, reproducing its step morphology, and the first 2 ML nuclei are visible. The preferential nucleation at step edges indicates that Mg atoms are highly mobile on the interface layer at this temperature (while they are trapped at

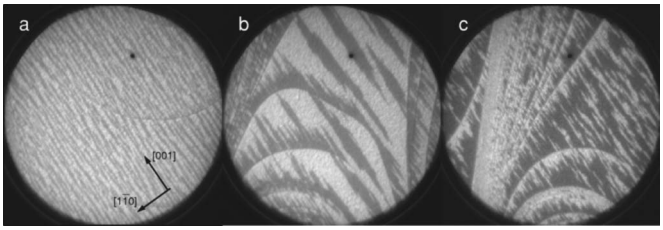

FIG. 2. LEEM images at 2.5 μm field of view: (a) second monolayer growth at 350 K, 0.1 ML/min. (b) 405 K, 0.12 ML/min, coverage 1.45 MLs. (c) Desorption at 450 K. The apparent change in orientation with respect to Fig. 1 is an effect of the electromagnetic lenses.

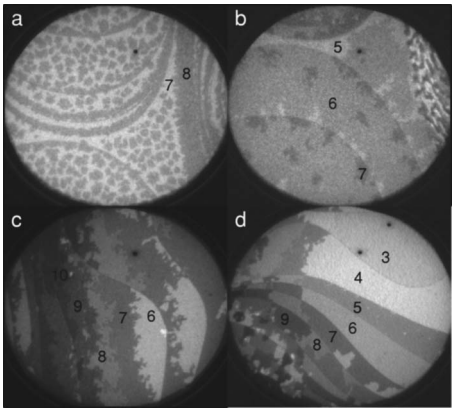

FIG. 3. LEEM images at different film growth stages. The number of atomic layers corresponding to each gray level is indicated. (a) 2.5 μm, 3.4 eV, 0.08 ML/min, and 350 K. (b) 2.5 μm, 3.4 eV, 0.085 ML/min, and 375 K. (c) 5 μm, 3.3 eV, 0.1 ML/min, and 390 K. (d) 5 μm, 1.1 eV, 0.2 ML/min, and 395 K.

steps), and that the surface defect density is extremely low. The relative density of nuclei at steps or on the terrace depends on the temperature. For $T>400$ K and flux $<\sim 0.1$ ML/min needles nucleate exclusively at steps, provided that the substrate surface is atomically clean, since even a small amount of impurities on the surface (due for example to pressures above 3×10^{-10} mbar during evaporation) increases the amount of nucleation centers on the terraces, giving rise to early coalescence of randomly distributed short needles and thus more irregular stripes.

The wires grow in length and width as more Mg is incorporated, always maintaining monoatomic height. In Figs. 1(e)–1(g) Mg coverages of about 1.1, 1.5, and 1.8 MLs are visible, with stripes from about 80 to 400 nm in width, reaching lengths of 3–4 μm. The highest aspect ratio, obtained for low wire density, is around 20. The morphology of this pattern is extremely sensitive to the growth parameters. Second layer Mg atoms are highly mobile at 405 K and even desorb, as evidenced by the fact that completion of the second monolayer takes almost twice as long as the first. In contrast, at room temperature the second monolayer grows *faster*, being less dense than the first one (see below). In Fig. 1(h) most of the surface is covered by the second Mg layer after coalescence of the different stripes, while some thin needlelike vacancy islands reveal the light interface monolayer, and the first dark islands of the third layer are visible at the step edges. These nuclei are only slightly elongated, and in fact, as growth proceeds and the film thickness increases, memory of the substrate symmetry is gradually lost.

As will be discussed below, the second monolayer atoms arrive on an interface Mg layer with nearly uniaxial strain, due to the anisotropic lattice mismatch between W(110) and Mg(0001). Thus both the adatom-adatom interaction and the diffusion are likely to be anisotropic. The size, density, and aspect ratio of the wires can be modified by varying the growth temperature, Mg coverage, and/or evaporation rate, and thus modifying the delicate balance between adsorption, desorption, and anisotropic diffusion. Some of the patterns obtained under slightly different conditions are illustrated in Fig. 2 (notice the field of view of only 2.5 μm). In all cases the wires have single atomic thickness, and correspond to 2 ML Mg (dark) on top of the wetting Mg monolayer (bright). For example, stripes grown at the same evaporation rate ($\approx$0.1 ML/min) but lower substrate temperature are more numerous, and reach about 1 μm in length with widths down to 30 nm, as visible in Fig. 2(a). The lower aspect ratio for higher temperature points to an anisotropic diffusion effect: assuming different energy barriers for diffusion along the two orthogonal directions, the diffusivity ratio $\sim e^{-E_d[001]/kT}/e^{-E_d[1\bar{1}0]/kT}>1$ decreases with temperature. On the other hand, growth at 405 K with a slightly higher deposition rate increases the probability of nucleation on terraces, as compared to migration and attachment to existing islands. On the larger terraces, many wires have coalesced to form pointed stripes with $\approx$1 μm length and a maximum width of $\approx$150 nm, and thus a smaller aspect ratio of 6–7:1 [Fig. 2(b)]. Finally, Fig. 2(c) illustrates how a striped pattern is obtained also by desorption of the second Mg monolayer: in this case wirelike vacancy islands nucleate, preferentially at step edges, and grow in length and width until the whole surface is 1 ML. It is also likely that at $T<350$ K wirelike growth takes place, with characteristic wavelengths below the LEEM lateral resolution ($\approx$10 nm).

Growth beyond the second monolayer proceeds in an approximately layer by layer fashion, where roughness increases with substrate temperature. Quantum size effects in LEEM give rise to energy dependent contrast between areas with different atomic thickness.[9] At and slightly above room temperature, the roughness is constant since ideal layer by layer growth takes place, with homogeneously distributed $N+1$ islands nucleating on each closed Nth atomic layer, as illustrated in the image of Fig. 3(a). Above about 350 K, mobility is high enough so that growth proceeds by step flow and thus the morphology is strongly dependent on the original substrate step landscape. The LEEM image in Fig. 3(b) nicely illustrates the asymmetry in the energy barrier for ascending and descending steps: growth fronts "ignore" downward step edges. Despite a residual tendency of nuclei to grow slightly faster along the bcc[001] direction, with increasing thickness the growth fronts tend to align with the direction of the steps, independently of their crystalline orientation. Larger and higher terraces show lower thickness and less thickness variation, as can be seen in Fig. 3(c). Finally in Fig. 3(d) it is shown how the substrate step land-

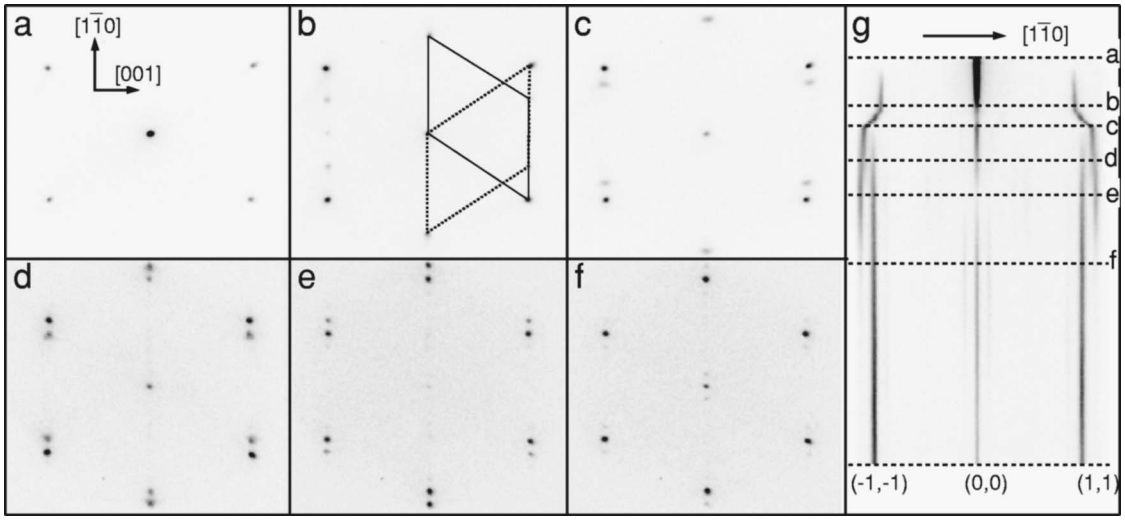

FIG. 4. LEED patterns from a Mg/W(110) deposition series at 390 K and 0.2 ML/min, at 26.3 eV. (a) Substrate, (b) 0.7 ML Mg: The unit cells from both domains are sketched, a multiple-scattering spot is visible in the center of each side line. (c) 1 ML Mg, (d) 1.5 ML Mg, (e) 2 ML Mg, (f) 3 ML Mg. (h) Profiles along the [1$\bar{1}$0] direction central line taken in ≈0.03 ML intervals, up to 6 ML Mg. The dotted lines indicate the coverage corresponding to patterns (a)–(f).

scape together with the step-crossing barrier asymmetry can be used to obtain borders between Mg areas of different thickness that are atomically straight over μm distances.

Desorption at moderate temperatures (400–450 K) of a multilayer Mg film takes place in a layer-by-layer fashion, in a process that is nearly mirrorlike of the growth one, including desorption of the second Mg monolayer by formation of vacancy needles and recovery of the striped pattern, as discussed above.

2. LEED

The structural evolution becomes clear analyzing the evolution of the LEED pattern. Figure 4 shows diffraction patterns illustrating the main stages of a growth series at 390 K. Figure 4(a) is the LEED pattern of the clean W(110) substrate. At this energy only the (0,0) spot and the (0,1) family spots are visible. From the beginning of evaporation, all substrate LEED spots decrease in intensity, indicative of an initially disordered phase but also of the lower electron reflectivity of Mg as compared to W. The substrate pattern remains otherwise unaltered. The (0,0) spot to background intensity ratio drastically decreases by a factor 20 up to 0.75 ML and then slightly recovers by somewhat less than a factor 2 upon the transition to the dense 1 ML phase, where it has a local maximum. From about 0.15 ML a new set of spots due to Mg is visible, indicating the formation of an ordered superstructure. This first submonolayer pattern, Fig. 4(b), is sharp since its appearance, and it corresponds to a distorted hexagonal Mg lattice in a Nishiyama-Wasserman (NW)-like configuration with the substrate, i.e., with the hexagonal base plane parallel to W(110), and the Mg most densely packed rows, hcp[11$\bar{2}$0], parallel to the W[001] direction. This orientation is natural[10] considering that the bulk lattice mismatch in this direction is only $(a_{\mathrm{Mg}}-a_{\mathrm{W}})/a_{\mathrm{Mg}}\approx 1.4\%$ while it is 19.5% in the perpendicular in-plane direction hcp[10$\bar{1}$0]‖bcc[$\bar{1}$10]. The unit cell of the Mg superstructure is a parallelogram with the short side aligned along the W[001] direction, and the long side along the substrate [1$\bar{1}$1] or [$\bar{1}$11] (by symmetry there are two possible orientational domains). The reciprocal unit cells are indicated in Fig. 4(b). The Mg-Mg distance coincides with the substrate lattice along [001] within experimental precision, and has a 3/4 coincidence with it along the long side of the parallelogram, i.e., three Mg atoms for every four W atoms. This corresponds respectively to −1.4% and +13.8% with respect to the relaxed bulk Mg lattice, and a 54.74° angle instead of 60°. The atomic density is 1.06×10^{15} cm^{-2}, about 6% lower than for bulk Mg.

The 3/4 pattern is maintained up to Mg coverage 0.75 ML, the spot intensity increasing with coverage. Growth of this superstructure proceeds thus in islands that coexist with the disordered phase and cover increasingly larger areas. This process implies an attractive Mg-Mg interaction, as has been also found for Mg on Ru(0001),[11] alkalis on Al(111),[12,13] and K on Ag(100),[14] in contrast to the "classical" picture of alkali adsorption. Calculations for alkalis on Al(111) have also shown a structural phase transition at $\theta\sim 0.1$,[15] as it becomes energetically favorable to alter the adsorbate-substrate interaction that gives rise to large dipoles for isolated atoms (and therefore dipole-dipole repulsion), and build up adsorbate islands with a metallic, attractive adsorbate interaction. This process can be considered a condensation of the Mg atoms. From the nucleation of this phase, the (0,1) family spots that had initially also drastically lost intensity, become more intense, since they now belong also to the Mg pattern, reaching a maximum at 1 ML Mg. As more Mg arrives on the surface, the overlayer undergoes a structural phase transition resulting in a lattice contraction along the W[1$\bar{1}$1] (or [$\bar{1}$11]) direction, while maintaining the orientation and the lattice coincidence with the substrate along W[001]. Figure 4(c) is the LEED pattern upon comple-

tion of the transition. In Fig. 4(g), profiles along the $[1\bar{1}0]$ central line extracted at close intervals during deposition, the fast lattice contraction is clearly visible as a strong outwards shift of the (1,1) and (−1,−1) spots. We have seen that at a slower deposition rate the change takes place in a narrower coverage range (roughly half the range or 0.1 ML for half the deposition rate), which points to a kinetic limitation. We have, however, not studied systematically this dependence. At saturation of the first monolayer, the 3/4 coincidence has evolved into 7/8; with a lattice constant of 3.13 Å in the W$[1\bar{1}1]$ direction, contracted by 2.5% with respect to the equilibrium distance (notice that before the lattice was expanded and thus the total contraction during the transition is more than 16%). The absence of multiple scattering spots in this pattern could mean that the superstructure is very close to a 7/8 coincidence but incommensurate or that there is some disorder. The atomic density of this phase is $\approx 1.24 \times 10^{15}$ cm^{-2} or 10.4% higher than in the bulk.

In contrast to the formation of the 3/4 structure, the transition from 3/4 to 7/8 coincidence lattices taking place between 0.75 and 1 ML is continuous, as demonstrated by the continuous simultaneous shift of all Mg LEED spots (and as will be seen, of the Mg 2*p* energy). The contraction occurs along the closest packed rows of the substrate, W$[1\bar{1}1]$ or $[\bar{1}11]$, where the W-W distance is only 2.74 Å. A strong anisotropy in adatom-adatom interactions due to the substrate atomic and electronic structure has been shown to lead to condensation in chains for several alkaline earths on furrowed metal surfaces such as W(112), Mo(112), or Re$(10\bar{1}0)$.[2] Typically initial adsorption takes place in lines normal to the furrow direction with large adatom-adatom separation. With increasing density, the overlayer is compressed along the furrows, going through a nonmetal to metal transition as a function of density. Although the W(110) surface does not present such pronounced furrows, the large Mg/W lattice mismatch in this direction provides a channel for easy compression, since the Mg can be considered as floating. Calculations have shown that differences in the adatom attractive interaction due to the substrate symmetry can be of the order of 0.1 eV/atom.[16] On more isotropic substrates such as Ru(0001), condensation in islands followed by compression was also observed, but in that case along all high-symmetry directions, and only up to the bulk Mg-Mg distance.[11] A closer look at Fig. 4(g) reveals that actually the LEED spots shift in a ratcheting manner, in the sense that there is a slight temporal locking of the pattern when passing through the 4/5 Mg/W coincidence (corresponding to the Mg-Mg distance 3.426 Å and equilibrium atomic density). It is likely that similar locking effects occur on passing through any commensurate relation with the substrate, the Mg-W interaction favoring configurations where one in every few atoms is in a minimum-energy adsorption site. In fact in an early LEED study, sharp 3/4, 4/5, and 5/6 patterns were observed as a function of Mg coverage,[17] and we have also observed them during monolayer desorption, where the higher temperature and slow coverage variation grant for better order. All Mg-related spots are in general very sharp, the widths only slightly higher than for the clean substrate spots. Only for some intermediate coverages, where fast changes take place (during the structural transitions), a Lorentzian broadening of the LEED peaks can be seen, indicative of disorder in the atomic arrangements. For completeness we note that the overall sub- and monolayer behavior is basically the same at room temperature, the main difference being that the Mg related spots are somewhat less sharp. This is true for both orthogonal directions and is mainly Gaussian broadening, and therefore related to a smaller island size rather than disorder in the Mg atomic positions within the islands. Slight variations have been found by varying the growth conditions, as, for example, Mg-W coincidence 4/5 instead of 3/4 before the fast compression for slower deposition and slightly lower temperature, but the general scheme is constant.

As soon as the second Mg monolayer nucleates a new set of weaker spots is visible. These are evident in the profiles of Fig. 4(g) as a pair of internal spots, coexisting with the interface ones. The new spots arise from diffraction from the 2 ML stripes, and are sharp since the beginning, with increasing intensity as larger areas are covered. Figure 4(d) is the pattern from 1.5 MLs, showing the coexisting 1 and 2 ML spots. The latter form a nearly undistorted hexagon with in-plane relaxed Mg lattice (within 1.4% in the Mg$[11\bar{2}0]\|$W[001] direction). Thus again at this interface, the lattice mismatch is anisotropic. The second monolayer atoms arrive on a surface that presents trenches of low corrugation potential along the W[001] direction, where all atoms are in low-energy adsorption sites, while along the orthogonal direction only one in every seven atoms is in such position. This is probably the origin of wirelike growth: it is responsible for anisotropic diffusion and also for anisotropic adatom-adatom interactions. The latter gives rise to what has been called anisotropic corner rounding,[18] i.e., a different probability for going around a corner, switching between island edges, depending on the orientation of the edges involved. This effect has been shown to be at least as important as anisotropic diffusion in determining island shape.[16,18,19] From about 1.5 ML coverage, the spots from the interface Mg layer slightly shift outwards by a further 3%, taking the correspondence Mg/W to 9/10, as can be clearly seen in Fig. 4(g). This new contraction provides at the same time a 8/9 coincidence between the second and the interface Mg atomic layers. Therefore the Mg-Mg interaction, competing with the Mg-W interaction is not enough to drive a full relaxation of the interface Mg layer, but enough to force it into commensurability (even at the cost of a higher compression) in order to allow coalescence of the stripes. The pattern of 2 ML Mg, Fig. 4(e), is a superposition of both sharp sets of spots from the interface and second monolayer, presenting also weaker but sharp multiple-scattering features. No further spot shifts are observed for subsequent Mg layers. In Fig. 4(f), from 3 ML Mg, the relaxed hexagon is the main pattern, but still multiple-scattering spots from the 8/9 coincidence with the interface layer are visible. It can be seen in Fig. 4(g) that although gradually attenuated, these persist up to several monolayers, and thus the atomic structure of the interface is preserved during the growth of subsequent layers, providing the buffer for an otherwise atomically abrupt transition be-

tween the W(110) and Mg(0001) lattices. The Mg multilayer spots are as sharp as those of the clean substrate.

The coverage dependent structural evolution described here is fully reversible. As mentioned above, desorption of a Mg multilayer at moderate temperatures proceeds layer by layer, starting from the highest thickness. After the second monolayer has completely desorbed, the interface atomic layer presents the same 7/8 LEED pattern from Fig. 4(c). With increasing temperature, the overlayer gradually loses density and sharp patterns corresponding to superstructures of 6/7, 5/6, 4/5, and 3/4 coincidence with the substrate can be clearly seen. The transitions between the different phases are continuous and the order is good. In fact, in all these cases sharp multiple-scattering spots are visible. Changes can be seen in LEED already from ~430 K, the dilute 3/4 superstructure is reached at ~630 K, and above that the Mg spots gradually weaken up to complete desorption at about 700 K.

B. Electronic structure of Mg/W(110): From adatoms to multilayer films

During the first stages of growth, the Mg $2p$ core level presents a series of shifts associated with the different structural phases. The evolution of the electronic structure will be presented and discussed in the following taking as reference the Mg $2p$ core-level energy from multilayer films. The multilayer Mg $2p$ spectrum is nicely fit with a single spin-orbit doublet at 49.8 eV binding energy. This is the same value as found for bulk samples within the scatter between different reports.[20–23] Also the spin-orbit splitting 0.27 eV, intensity ratio 0.5, and asymmetry $\alpha=0.13$ agree with the Mg bulk values.[20,21] A Gaussian broadening around 0.27 eV was used consistently throughout the data sets, derived from the overall experimental resolution and phonon broadening (the spectra were taken during growth and thus at temperatures typically around 350–400 K). The multilayer Mg $2p$ peak has a Lorentz width of 0.1 eV, equal to the reported Mg surface value and slightly higher than the bulk one (0.07 eV). Our spectra did not require an extra surface component as has been found in high-resolution photoemission spectra of polycrystalline Mg films [$\Delta E_B=0.14$ eV (Ref. 20)] and bulk Mg($1\bar{1}00$) samples [$\Delta E_B=0.19$ eV (Ref. 21)], as neither did spectra from thin Mg(0001) films on Mo(001).[24] There is, to the best of our knowledge, no high-resolution core-level spectroscopy report of the (0001) surface of bulk Mg that could provide a direct comparison, which makes it speculative at this point to discuss eventual differences. It could well be that the surface core-level shift is too small to be relevant at our energy resolution.

Figure 5(a) shows the evolution of the Mg $2p$ core level as a function of coverage during deposition at 390 K. A close look at the spectrum for the lowest coverage reveals a tiny but clear peak that appears immediately upon initial Mg adsorption, at a binding energy of 49.9 eV and thus $\Delta E_B=0.1$ eV with respect to the multilayer (marked by a tick in the graph). LEEM images show an excellent surface quality, and permit selecting microspot areas with extremely low step density (typically one or two atomic steps in the whole 3 μm^2 area). Since at this temperature there is adsorption on the terraces and not only at step edges, the contribution to the photoemission signal from adatoms at steps or defects should be negligible in our sampling area. This component is thus assigned to isolated Mg adatoms in a disordered disperse phase. The peak has a width of ≈1 eV and reaches a maximum intensity at 0.15 ML, when a new core-level component appears at $\Delta E_B=-0.45$ eV. This new interface component is assigned to emission from the 3/4 phase, since it appears exactly when the 3/4 LEED spots start being visible, and stays at constant energy while gaining intensity with coverage, up to 0.75 ML, as do the diffraction spots. This evolution, highlighted by a dashed line in Fig. 5(a), is in agreement with the picture of condensation and growth in islands with local 3/4 structure, i.e., Mg lattice uniaxially expanded. In fact, our fits reveal that both components coexist in the 0.15–0.75 ML range, as visible in the 0.5 ML spectrum of Fig. 5(b), the area of the disperse phase remaining constant up to ~0.5 ML, and rapidly losing intensity above that, as the dispersed phase area decreases at the expense of the condensed phase. Further temperature-dependent measurements would be necessary in order to tackle the phase diagram of this low coverage range and in particular the limits for coexistence of the disperse and condensed phases. With further coverage, continuing in clear correlation with the LEED pattern evolution for growth at the same temperature and rate, the interface Mg $2p$ shifts during the lattice contraction (0.75–1 ML), reaching the monolayer value $\Delta E_B=-0.6$ eV when the transition to the 7/8 lattice is complete: a −0.15 eV shift thus upon a 16.3% lattice contraction. Despite the fact that lattice matching at the interface necessarily requires several nonequivalent adsorption sites, both the 3/4 and 7/8 phase core-level fits require a single spin-orbit doublet, as visible in the fit of 1 ML Mg in Fig. 5(b). Thus the energy variations due to different local bonding environments are small compared to our energy resolution. This behavior of the interface component is the same as observed for alkali/d-metal,[25–27] alkali/sp-metal,[13] and Ba/W[28] interfaces, including the sign and magnitude of the shift for the saturated monolayer, while slight positive E_B shifts have been reported for Mg adsorption on Mo(100)[24] and Ru(0001).[29]

An interface component is also evident in the W $4f$ spectra. In Fig. 5(c) the core level of the clean W(110) surface is compared to those covered by a submonolayer and monolayer amounts of Mg. At first the surface component is attenuated and then an interface component grows, clearly due to the interaction with Mg, since it persists until long after the entire surface is covered by it. The W $4f$ interface component is at 0.35 eV lower binding energy than the bulk peak, thus only −0.03 eV with respect to the W(110) surface component for the clean surface, at −0.32 eV,[30] similar values as those found for alkalis on d metals,[25,26] and for Ba/W(110).[28]

The shift of the 3/4 to *lower* binding energy with respect to the multilayer peak cannot be explained in a simple charge-transfer picture, which would imply transferring electrons to the more electropositive element. In fact, this considerable shift is of the same sign and order of magnitude as those of most alkali/d- and sp-metal systems[13,25–27] as well

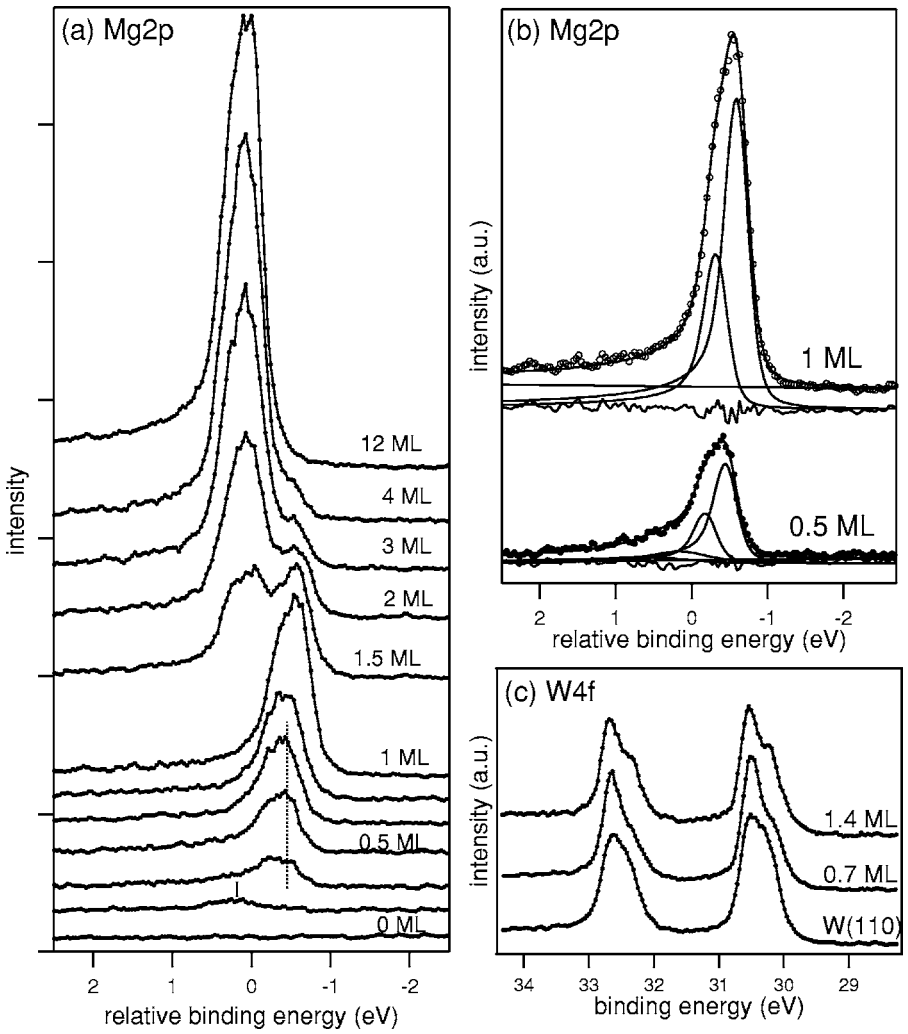

FIG. 5. μXPS spectra at different Mg coverages. (a) Mg $2p$ core level, hν=112 eV. (b) Fit of the 1 ML and 0.5 ML spectra: data, fit, separate spin-orbit components, and residuum. (c) W $4f$ core level, hν=168 eV.

as Ba/W(110).[28] This kind of behavior, together with surprisingly small shifts of the substrate core level, were invoked in the early 1990s to dismiss the classical charge transfer picture of alkali adsorption.[25] Rather, photoemission results were explained within a thermodynamic model[31,26,27] where the interface core-level shift can be approximately understood as the interface segregation energy of a Z+1 impurity (in this case Al) from the Mg bulk to the Mg/W interface. While this interpretation remains valid, after the initial controversy[30,32] the combined efforts of different research groups worldwide lead to a picture of alkali adsorption compatible both with the experimental core-level shifts and with the charge-density changes predicted by theory,[33,34] where the bonding can still be described as ionic in the low coverage limit. Shortly, isolated adatoms are partially polarized, and screening by the metal substrate results in an increased electron density in the interface region (image plane). The concept of interstitial charge at the image plane is of course only valid for large atoms that are far enough from the surface.

When the Mg coverage increases the attractive adsorbate-adsorbate interaction sets in, dominating over the adsorbate-substrate interaction, depolarizing the adatoms. The −0.55 eV energy shift of the condensed 3/4 phase with respect to the dispersed one indeed supports this picture and gives an idea of the relative importance of both effects. This new component appears abruptly, coexists with the +0.1 eV peak at the beginning, and gains intensity with coverage, just as our structural data show that condensation occurs in the form of an abrupt phase transition, and islands of the condensed phase occupy increasingly larger surface areas. In other words, there is a transition from a bondlike (localized) to a bandlike (delocalized) electronic phase in the Mg overlayer, possibly related to a nonmetal-to-metal transition as has been found in valence-band and photoelectron yield studies of several alkali and alkaline-earth overlayers on metals as a function of (submonolayer) coverage.[2] The further gradual shift to lower binding energy observed between 0.75 and 1 ML, with increasing atomic density, is a general feature of submonolayer alkali and alkaline earths. The electronic charge density on the atoms increases for higher coordination, leading to both a core-level shift to lower binding energy and a more effective screening of the core hole. The negative Mg $2p$ core-level shift of the saturated monolayer, while it is positive for adsorption on Mo(100)[24] or Ru(0001),[29] could indicate a weaker interaction at the Mg/W(110) interface, supported by the fact that the interface layer is pseudomorphic on Mo(100)[23] and by the higher desorption temperature on Ru(0001).[11] The Mg $2p$ peak of the saturated monolayer has only slightly higher linewidth

(about 0.03 eV) than that of the multilayer peak, while a slight increase for submonolayer coverage, with a maximum at 0.15 ML (+0.1 eV), can be assigned to phonon broadening due to increased vibrational freedom.

Within experimental precision there are no further shifts of the interface Mg 2*p* upon nucleation, growth, and coalescence of the second monolayer. Rather, a new component appears with a binding energy of 49.8 eV, and coexists with the interface component, as can be seen in the spectra of 1.5 and 2 MLs of Fig. 5(a). The new component already has the energy and linewidth of the core level for multilayer films, and simply increases intensity with further deposition, while the interface component is exponentially attenuated. Very similar spectra are obtained for other growth conditions in the studied range, independent of the details of the wires morphology.

The valence-band spectra for low Mg coverage are dominated by emission from the substrate in the photon energy range available during experiment and thus not shown here. No clear Mg-related state could be detected in the striped phase spectra. Compared to the valence band of clean W(110), the main differences are that the peak at $E_B = 1.4$ eV (emission from tungsten Σ_5 band edge), is broadened due to a Mg contribution on the high E_B side, probably the precursor of the Mg(0001) surface state that develops at 1.6 eV for thicker films, and that the intensity at the Fermi energy is relatively stronger, what can be assigned to emission from the Mg *s-p* band. Specific angle-resolved photoemission studies could reveal interesting phenomena arising from varying density in the interface Mg layer [such as the nonmetal-metal transition observed in Mg submonolayers on Mo(112) and Re(10$\bar{1}$0)[2]] or from the striped morphology at $1+x$ ML coverages, possibly giving rise to quasi-one-dimensional electronic states. Valence-band spectra from multilayer films present the characteristic Mg(0001) surface state at 1.6 eV binding energy, and thickness dependent quantum-well states in the Mg *s-p* band due to electron confinement to the overlayer.[6,7]

IV. SUMMARY AND CONCLUSIONS

Nearly perfect layer by layer growth and desorption in the room temperature to 450-K range permit us to obtain a rich variety of low-dimensional structures in the Mg/W(110) system. In the initial stages of adsorption, a Mg 2*p* peak due to emission from isolated adatoms is identified, as well as another strongly shifted component as soon as condensation in islands starts. When all the surface is covered by the first condensed superstructure, where the Mg-Mg distances are expanded with respect to the bulk value, a continuous lattice contraction takes place in the overlayer along one of the crystalline directions, correlated with a further core-level energy shift, until an anisotropically strained overdense Mg monolayer is formed. Self-organized monolayer height mesoscopic wires of various sizes and shapes can be grown on top of the interface Mg layer, by tuning the growth and annealing parameters. The resulting surfaces consist of the combination of areas of one and two monolayers of Mg on top of an electron-reflecting substrate. The areas have distinctly different electronic as well as structural properties, representing thus an ideal template for further deposition of nanostructures and adsorption studies. Thanks to the clear LEED and Mg 2*p* fingerprints of the different phases, angle-resolved valence-band photoemission spectra with high-energy resolution could be performed in order to tackle the eventual existence of nonmetal-to-metal transition during submonolayer condensation, and confined one-dimensional electronic states in the striped phase.

ACKNOWLEDGMENTS

We thank S. Heun for his help during part of the measurements. L. Aballe acknowledges support from the European Community.

*Present address: ALBA Synchrotron Light Facility, Edifici Ciències Nord. Mòdul C-3 central, Campus Universitat Autònoma de Barcelona, 08193 Bellaterra, Barcelona, Spain. Email address: lucia.aballe@cells.es

[1] See, for example, T.-C. Chiang, Surf. Sci. Rep. **39**, 181 (2000); K. De'Bell, A. B. MacIsaac, and J. P. Whitehead, Rev. Mod. Phys. **72**, 225 (2000); F. J. Himpsel, J. Phys.: Condens. Matter **11**, 9483 (1999), and references therein.

[2] I. N. Yakovkin, G. A. Katrich, A. T. Loburets, Y. S. Vedula, and A. G. Naumovets, Prog. Surf. Sci. **59**, 355 (1998), and references therein; P. A. Dowben, Surf. Sci. Rep. **40**, 151 (2000), and references therein; G. A. Katrich, V. V. Klimov, and I. N. Yakovkin, J. Electron Spectrosc. Relat. Phenom. **68**, 369 (1994); J. Zhang, D. N. McIlroy, and P. A. Dowben, Phys. Rev. B **49**, 13780 (1994); **52**, 11380 (1995).

[3] L. Wallden, Phys. Rev. Lett. **54**, 943 (1985); E. W. Plummer and P. A. Dowben, Prog. Surf. Sci. **42**, 201 (1993), and references therein; S. R. Barman, K. Horn, P. Haberle, H. Ishida, and A. Liebsch, Phys. Rev. B **57**, 6662 (1998), and references therein; L. Aballe, C. Rogero, and K. Horn, Surf. Sci. **518**, 141 (2002).

[4] L. Aballe, C. Rogero, and K. Horn, Phys. Rev. B **65**, 125319 (2002).

[5] F. Schiller, M. Heber, V. D. P. Servedio, and C. Laubschat, Phys. Rev. B **70**, 125106 (2004); C. Koitzsch, C. Battaglia, F. Clerc, L. Despont, M. G. Garnier, and P. Aebi, Phys. Rev. Lett. **95**, 126401 (2005); F. Schiller, R. Keyling, E. V. Chulkov, and J. E. Ortega, *ibid.* **95**, 126402 (2005).

[6] L. Aballe, A. Barinov, A. Locatelli, S. Heun, and M. Kiskinova, Phys. Rev. Lett. **93**, 196103 (2004).

[7] T. Schmidt, S. Heun, J. Slezak, J. Diaz, K. C. Prince, G. Lilienkamp, and E. Bauer, Surf. Rev. Lett. **5**, 1287 (1998); A. Locatelli, L. Aballe, T. O. Mentes, M. Kiskinova, and E. Bauer, Surf. Interface Anal. **38**, 1554 (2006).

[8] D. L. Adams and J. N. Andersen, FitXPS package, http://www.sljus.lu.se/download.html

[9] M. S. Altman, W. F. Chung, Z. Q. He, H. C. Poon, and S. Y. Tong,

Appl. Surf. Sci. **169-170**, 82 (2001).
[10] E. Bauer and J. H van der Merwe, Phys. Rev. B **33**, 3657 (1986).
[11] H. Over, T. Hertel, H. Bludau, S. Pflanz, and G. Ertl, Phys. Rev. B **48**, 5572 (1993).
[12] A. Hohlfeld and K. Horn, Surf. Sci. **211/212**, 844 (1989).
[13] J. N. Andersen, E. Lundgren, R. Nyholm, and M. Qvarford, Surf. Sci. **289**, 307 (1993).
[14] S. Modesti, C. T. Chen, Y. Ma, G. Meigs, P. Rudolf, and F. Sette, Phys. Rev. B **42**, 5381 (1990).
[15] J. Neugebauer and M. Scheffler, Phys. Rev. Lett. **71**, 577 (1993).
[16] A. Locatelli, C. Sbraccia, S. Heun, S. Baroni, and M. Kiskinova, J. Am. Chem. Soc. **127**, 2351 (2005).
[17] D. A. Gorodetsky and Fung Ho, Ukr. Fiz. Zh. (Russ. Ed.) **14**, 94 (1969).
[18] Y. Li, M. C. Bartelt, J. W. Evans, N. Waelchli, E. Kampshoff, and K. Kern, Phys. Rev. B **56**, 12539 (1997).
[19] Z. Zhang and M. G. Lagally, Science **276**, 377 (1997).
[20] R. Kammerer, J. Barth, F. Gerken, C. Kunz, S. A. Flodstrom, and L. I. Johansson, Phys. Rev. B **26**, 3491 (1982).
[21] P. A. Thiry, J. Ghijsen, R. Sporken, J. J. Pireaux, R. L. Johnson, and R. Caudano, Phys. Rev. B **39**, 3620 (1989).
[22] X. D. Peng and M. A. Barteau, Surf. Sci. **233**, 283 (1990).
[23] V. Fournier, P. Marcus, and I. Olefjord, Surf. Interface Anal. **34**, 494 (2002).
[24] J. W. He, J. S. Corneille, and D. W. Goodman, Appl. Surf. Sci. **72**, 335 (1993).
[25] D. M. Riffe, G. K. Wertheim, and P. H. Citrin, Phys. Rev. Lett. **64**, 571 (1990).
[26] E. Lundgren, M. Qvarford, R. Nyholm, J. N. Andersen, and D. Heskett, Phys. Rev. B **50**, 4711 (1994).
[27] M. L. Shek, J. Hrbek, T. K. Sham, and G. Q. Xu, Phys. Rev. B **41**, 3447 (1990).
[28] T. W. Pi, I. H. Hong, and C. P. Cheng, Phys. Rev. B **58**, 4149 (1998).
[29] H. H. Huang, X. Jiang, H. L. Siew, W. S. Chin, W. S. Sim, and G. Q. Xu, Surf. Sci. **436**, 167 (1999).
[30] D. M. Riffe, G. K. Wertheim, and P. H. Citrin, Phys. Rev. Lett. **63**, 1976 (1989).
[31] B. Johansson and N. Maartensson, Phys. Rev. B **21**, 4427 (1980).
[32] H. Ishida, Phys. Rev. B **38**, 8006 (1988); M. Scheffler, C. Droste, A. Fleszar, F. Maca, G. Wachutka, and G. Barzel, Physica B **172**, 143 (1991); X. Shi, D. Tang, D. Heskett, K. D. Tsuei, H. Ishida, Y. Morikawa, and K. Terakura, Phys. Rev. B **47**, 4014 (1993).
[33] J. Bormet, J. Neugebauer, and M. Scheffler, Phys. Rev. B **49**, 17242 (1994).
[34] P. S. Bagus and G. Pacchioni, J. Chem. Phys. **102**, 879 (1995).